Discover Chemistry

Research

Enhanced solar photodegradation of reactive blue dye using synthesized codoped ZnO and TiO_2

Zeinab A. Suliman[1,2] · **Achisa C. Mecha**[3,4] · **Josphat I. Mwasiagi**[1,5]

Received: 4 November 2024 / Accepted: 24 February 2025
Published online: 10 March 2025

Abstract
The rapidly growing textile industry produces various textiles, which has led to significant water pollution due to the discharge of dyes and chemicals. In this study, TiO_2 doped ZnO photocatalyst was synthesized and characterized to determine the morphology and composition (scanning electron microscopy, SEM&EDX), optical properties (ultraviolet–visible diffuse reflectance spectroscopy, UV DRS), functional groups (Fourier Transform Infrared spectroscopy), and crystal structure (X-ray diffraction). The photocatalysts were used to photodegrade reactive blue dye in aqueous solution (1–3 mg/L) under natural sunlight. The SEM showed agglomerated granular particles, with increased agglomeration and smaller particle size for lab-synthesized TiO_2 (TZT) compared to commercial TiO_2 (TZC). The EDX results confirmed the presence of only Ti, Zn, and O in both photocatalysts, signifying the presence of ZnO and TiO_2 and the absence of contamination. The UV DRS revealed a reduction in band gap from 3.6eV (ultraviolet light region) to 3.02eV (visible light region). At a dye concentration of 1 mg/L, 0.03 mg of photocatalyst, and a pH of 5, under sunlight, the degradation efficiencies were 86.9% for ZnO, 91% for TZC, and 100% for TZT. The rate constants (k) were 0.01203, 0.01511, and 0.08261 min-1 for bare TiO_2, TZC, and TZT, respectively. The photocatalysts were recovered and reused over five consecutive cycles without significant reduction in performance, thus confirming the stability and durability of the TiO_2-ZnO photocatalysts (TZT and TZC). The lab-synthesized photocatalysts demonstrated superior performance (100% degradation) and the utilization of natural sunlight which is green energy contributes to a clean and sustainable environment.

Keywords Doping · Photocatalyst · Visible light · Sunlight · Water pollution · Degradation efficiency

1 Introduction

Nanoscience is a rapidly evolving field with widespread appeal across scientific disciplines. It studies three-dimensional materials at the nanometer scale (dimensions ranging from 1 to 100 nm) or possessing at least one dimension within this range [1, 2]. The diverse behaviors of nanoparticles and nano photocatalysts, influenced by factors such as size, shape, charge, and surface area, make them versatile tools with significant potential in various applications [3]. One notable application is their ability to effectively degrade organic pollutants found in wastewater arising from textiles, paper, and plastics industries which pose considerable threats to human health and the environment [4]. When harnessed

✉ Zeinab A. Suliman, zoba23165@gmail.com | [1]Department of Manufacturing, Industrial and Textile Engineering, Moi University, Eldoret, Kenya. [2]Renewable Energy, Nanomaterials and Water Research Group, Department of Chemical Engineering and Technology, Gezira University, Wad Madani, Sudan. [3]Renewable Energy, Nanomaterials and Water Research Group, Department of Chemical and Process Engineering, Moi University, Eldoret, Kenya. [4]Department of Environmental Science, University of Arizona, Tucson, USA. [5]Departmeent of Technology Education, Open University of Kenya, Konza, Kenya.

appropriately, nanoparticles offer promising solutions for the removal of pollutants such as pharmaceuticals [5], pesticides [6], phenols and acid [7], and dyes [8–10] from industrial wastewater effluents [11].

The TiO_2 photocatalyst is widely used for degrading organic and inorganic pollutants from water [12]. The photocatalyst performance is attributed to its high stability, low cost, low toxicity, and superior photocatalytic activity compared to other semiconductor materials [13]. Despite these benefits, TiO_2 primarily exhibits photocatalytic activity in the ultraviolet (UV) region, constituting only about 5% of the Earth's solar spectrum. Consequently, its effectiveness in the visible range is limited [11], TiO_2 exists in three phases, anatase, rutile and brookite; of these, anatase is considered the most photoactive form. Anatase has strong adsorption of organic compounds and high hole trapping rate; however, rutile and brookite phases also exhibit considerable photoactivity. Incorporating multiple phases of TiO_2 enhances photocatalytic performance and diminishes charge carrier recombination. Anatase is the most thermally stable crystal phase of TiO_2; annealing it at temperatures exceeding 400°C can transform it to rutile [14, 15]. Similarly, zinc oxide (ZnO) serves as a photocatalyst due to its potent oxidizing capabilities, non-toxic nature, and cost-effectiveness [16]. ZnO exhibits diverse nanostructures, such as nanoneedles and nanocombs [17].The photocatalytic properties of ZnO can be enhanced by doping [18] since ZnO has a wide band-gap [19, 20].

The modification of photocatalysts such as TiO_2 or ZnO often employs doping techniques [21], such as metal oxide doping. A study by [22] aimed at enhancing photocatalytic properties by reducing the recombination rate of photoinduced electrons and holes, thereby improving the overall efficiency of the photocatalyst. By integrating both TiO_2 and ZnO and employing this dual doping strategy, it is possible to leverage the advantages of each while mitigating their respective drawbacks [23].

The photocatalytic process employed in water treatment effectively breaks down various organic substances, encompassing alkanes, lipids, organic acids, aromatics, dyes, and other compounds. These pollutants undergo systematic oxidation, resulting in the formation of low molecular weight intermediates which can be further oxidized, ultimately transforming into environmentally benign byproducts such as carbon dioxide (CO_2), water (H_2O), and other anions [24], Photodegradation contributes to the effective removal and transformation of organic contaminants, promoting the purification of water resources. Studies on photocatalytic degradation of dyes has been reported, such as reactive blue dye [25], different reactive dyes [26], Orange II dye [27], using pure TiO_2 under UV light, and methylene blue under visible light by dye sensitized titania [28], also reactive blue 203 dye using ZnO nanoparticles [29]. However, all these studies evaluated the performance of TiO_2 and ZnO separately. There is a need to assess the performance of co-doped TiO_2 and ZnO to elucidate synergistic effects.

The novelty of this study is that it performed a comparative analysis of lab synthesized co-doped TiO_2-ZnO photocatalysts and ZnO co-doped with commercial TiO_2. The co-doping was done to shift the light absorption to the visible light region and enable the utilization of natural sunlight. The lab synthesized photocatalyst demonstrated superior performance that illustrated effective visible light absorption. The study also evaluated the recovery and reuse of the photocatalyst at least five times without significant reduction in performance, showing their stability and durability. Solar photocatalysis offers a cost-effective, eco-friendly water treatment technology; it eliminates the use of electricity (UV lamps and pumps).

2 Materials and methods

2.1 Materials

Zinc acetate dehydrate ($Zn(CH_3COO)_2.2H_2O$, 98.0%), sodium hydroxide (NaOH), acetone, titanium dioxide (TiO_2) powder, and absolute ethanol (C_2H_5OH, 99.0%), were obtained from DLA Chemical Reagent Company, Titanium(IV) tetraisopropoxide 97% (TTIP, Aldrich), Reactive navy blue HER dyes from Rivatex Ltd. The reagents were of analytical grade and were used without further purification. Deionized water, sourced from Eldo Chemical Reagent Company, was employed for all synthesis and treatment procedures.

2.2 Preparation of the samples

2.2.1 Synthesis of TiO_2

The TiO_2 powder was prepared through sol–gel method as reported by [30]. Initially, 55 ml of ethanol, 135 ml of deionized (DI) water, and 0.2 ml of acetic acid were combined. Then, 18.5 ml of tetraisopropoxide was gradually added to the solution, which was stirred with a magnetic stirrer for 48 h. The resulting precipitate was filtered, washed with DI water, and dried at 80 °C for 24 h. After drying, the material was calcined at 500 °C for 2 h, and the agglomerate was finely ground using a mortar and pestle to produce TiO_2 powder.

2.2.1.1 Doping of synthesized and commercial TiO_2 by ZnO The ZnO doping of both commercial TiO_2 and lab-synthesized TiO_2 was carried out using the sol–gel method, as described by [18]. In this process, 25 ml of 0.01 mol TiO_2 nanopowder was combined with 25 ml of zinc-acetate dehydrate, with the mixture stirred magnetically at 80 °C for 6 h. Once cooled to room temperature, the pH was adjusted to 11.5 by gradually adding 10 ml of 1 M sodium hydroxide dropwise. The mixture was further stirred at 60 °C for 60 min. The resulting gel was washed with deionized water, dehydrated at 105 °C, and calcined at 550 °C for 3 h. The final TiO_2/ZnO photocatalyst (referred to as TZT for synthesized TiO_2 and TZC for commercial TiO_2) was obtained by grinding the agglomerate with a mortar and pestle.

2.3 Photocatalyst characterization

The photocatalysts were characterized to determine the functional groups using Fourier transform-infrared Spectroscopy (FTIR) using a Perkinelmer Frontier instrument in ATR mode, covering the spectral range from 4000 to 650 cm^{-1} to elucidate the chemical compositions of their surfaces. The surface morphologies of the photocatalysts were examined using Scanning Electron Microscopy (SEM) on a Zeiss Ultra55, with Energy-dispersive X-ray analysis (EDX) providing additional insights into the chemical makeup of the photocatalyst nano powder. The structural characteristics of the photocatalyst TiO_2 and ZnO nano powder were determined through X-ray Diffraction using a Smartlab X-Ray Diffractometer, with PXRD, HRXRD, XRR capability. Furthermore, the optical properties of the photocatalyst were assessed via UV Diffuse Reflectance Spectroscopy (UV DRS) to determine light absorption in the visible region.

2.4 Photocatalytic degradation of reactive blue dye

Six reaction tubes for each type of ZnO/TiO_2 photocatalyst, containing reactive blue dye at concentrations of 1, 2, and 3 mg/L were used. These solutions were mixed with 0.02 gm ZnO-TiO_2 photocatalyst nano powder and exposed to sunlight for 2 h with periodic stirring every 15 min to investigate the impact of the light irradiation on dye removal. Samples were drawn and analyzed using UV–Vis spectrophotometry at $\lambda_{max} = 600$ nm to assess the degradation of the blue dye and the degradation efficiency (DE) % determined using equation

$$\text{DE}\ (\%) = \frac{C_0 - C_t}{C_0} \times 100\% \tag{1}$$

where: C_o and C_t represent the initial and final concentrations of Reactive blue dye by (mg/l) respectively.

From the plot of ln(C/C0) verses sunlight irradiation time, the rate constant, k, is calculated using Eq. (2) [31]:

$$Ln\frac{C}{C_0} = -k.t \tag{2}$$

where t is the time of sunlight irradiation.

The impact of TZT and TZC photocatalyst concentrations on blue dye removal was investigated using a concentration range of 0.01–0.03 mg/L. A 1 mg/L blue dye solution at a pH of 6.5 was irradiated for 2 h. Afterward, the samples were analyzed with UV–Vis spectrophotometry to determine the dye degradation efficiency based on Eq. 1.

Since pH is a critical factor in dye removal, the pH of the 1 mg/L dye solution was adjusted within the range of 5 to 9 by carefully adding 0.1 M HCl and NaOH solutions. Following the pH adjustment, 0.02 mg/L of each photocatalyst was added to 20 mL of the dye solution at each pH level. The mixtures were then subjected to sunlight irradiation for 2 h,

and the degradation efficiency was assessed using UV–Vis spectrophotometry. The specific experimental parameters, pH range, photocatalyst dosage, dye concentration and reaction time, were selected based on prior studies [26, 29] and practice to get optimum value.

2.5 Photocatalyst stability

Evaluating the performance of nanophotocatalysts in various applications and ensuring the economic feasibility of the photodegradation process require key considerations such as durability and ease of recovery. This study investigates the TiO_2-ZnO nanophotocatalyst over five cycles, highlighting its distinctive pollutant removal method that avoids chemical treatments. The recovery process involves allowing the solution to settle for several hours, followed by water separation and drying the material at 60 °C, as described in [32].

3 Results and discussion

3.1 Characterization of the photocatalysts

3.1.1 FTIR analysis

Figure 1 shows the FTIR spectrum revealing minor peaks at 3438 cm^{-1} and 1460 cm^{-1} for ZnO, and 3390 cm^{-1} and 1626 cm^{-1} for TiO_2. This indicates the presence of –OH group stretching vibrations and H–O–H bond deformation attributed to trace amounts of adsorbed water on their surfaces, in agreement with the literature [33]. For TiO_2, the FTIR spectrum displays a wide band from 472 to 880 cm^{-1}, resulting from the overlap of Ti–O–Ti and Ti–O vibration modes. The prominent peak at 672 cm^{-1} is attributed to Ti–O stretching. The H–O–H and O–H stretching and bending vibrations produce signals in the ranges of 2852–3800 cm^{-1} and 1600–1682 cm^{-1}, respectively, indicating negligible moisture content in all photocatalysts [10]. No additional peaks are detected in the FTIR spectra, confirming the absence of contamination in each photocatalyst.

3.1.2 SEM analysis

The SEM images shown in Fig. 2 reveal that both the undoped TiO_2 (Fig. 2 a) and TiO_2-ZnO nanoparticles (Fig. 2b, c) display irregular shapes and sizes. It appears that small, spherical particles have combined to form larger, irregular agglomerates. This behavior is commonly observed in TiO_2 nanoparticles and has been documented by other researchers [34, 35]. The agglomeration occurs as a result of the tiny particle size, leading to the fusion of particles into clusters [36]. In Fig. 2b, c in addition of TiO_2 the ZnO was clearly appear in the images. The observed distribution of elements such as Zn, Ti, and O across the sample confirmed their uniform presence, providing validation for the successful synthesis of

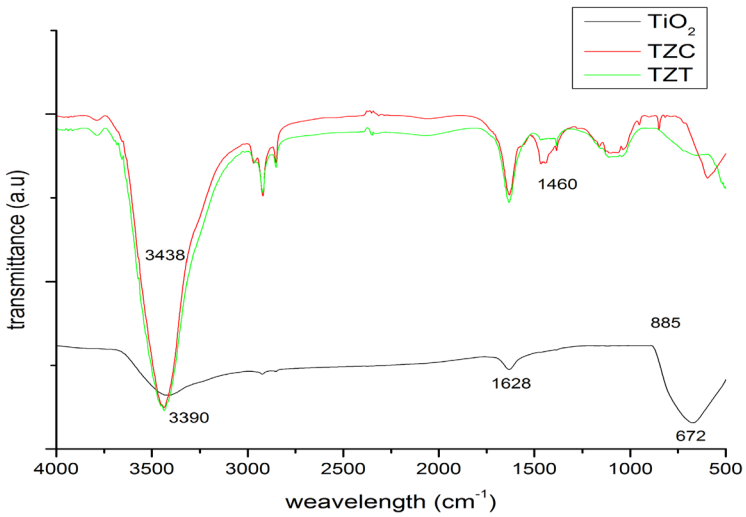

Fig. 1 FTIR spectra of TiO_2, TZC, and TZT photocatalysts

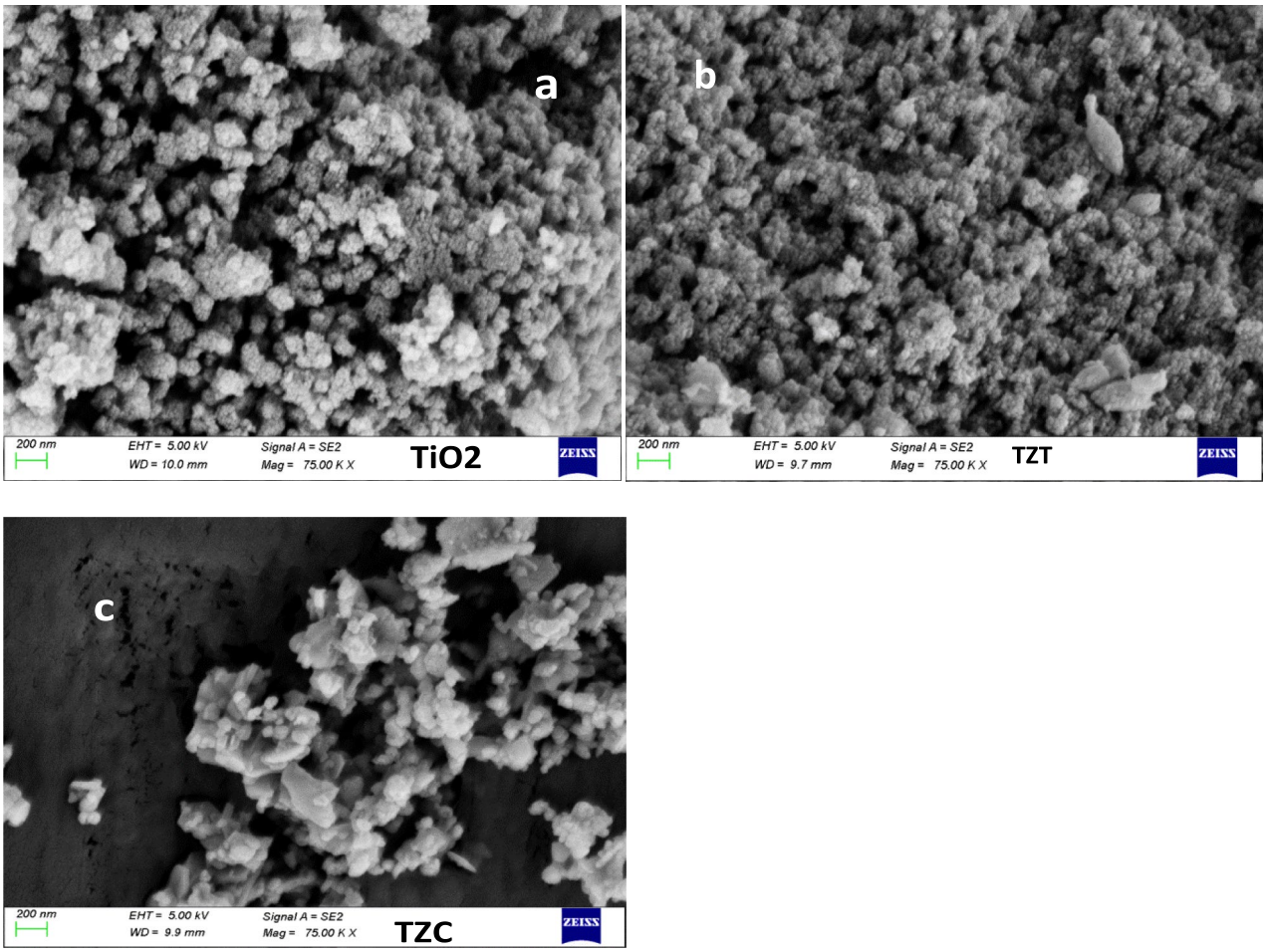

Fig.2 SEM images of **a** TiO_2, **b** TZT, and **c** TZC photocatalysts

ZnO-TiO_2 nanocomposites. Notably, particles of ZnO-TiO_2 produced from synthesized TiO_2 (Fig. 2b) exhibited a tendency to agglomerate more than particles of ZnO-TiO_2 (Fig. 2c) produced from commercial TiO_2, as evident in the SEM images.

3.1.3 EDX analysis

EDX analysis results for TZT and TZC are shown in Fig. 3a, b and Fig. 3c, d, respectively. The EDX spectra depicted specific peaks indicating the presence of Ti, O, and Zn atoms in the mixed oxide nanocomposite samples. The elemental composition portrayed in the spectrum corresponds with the various stages of Zn-TiO_2 photocatalyst preparation, illustrating the successful integration of zinc into the titanium dioxide structure. No other components were observed thereby confirming the absence of impurities.

3.1.4 XRD analysis

XRD analysis results are depicted in Fig. 4a, b; Fig. 4a shows the XRD patterns of synthesis TiO_2, the XRD pattern of ZnO displays well-defined diffraction peaks at 2θ values of 25.28, 37.8, 48.05, 53.89, 55.06, 62.69, 68.67, 70.31, and 75.03 These characteristic peaks are attributed to the (101), (004), (200), (105), (211), (204), (116), (220), and (215) crystallographic planes, respectively, aligning with the wurtzite hexagonal phase of Reference: TiO_2 antase Natl. Bur. Stand. (U.S.) Monogr. 25 7(1969)82. Figure 4b a TiO_2-ZnO photocatalysis shows the XRD pattern of ZnO displays well-defined diffraction peaks at 2θ values of 31.65, 34.18, 36.05, 47.12, 56.34, 62.74, 66.35, 67.84, 69.04, 72.58, and 76.95. These characteristic peaks are attributed to the (100), (002), (101), (102), (110), (103), (200), (112), (201), (004), and (202) crystallographic planes, respectively, aligning with the wurtzite hexagonal phase of ZnO (JCPDS

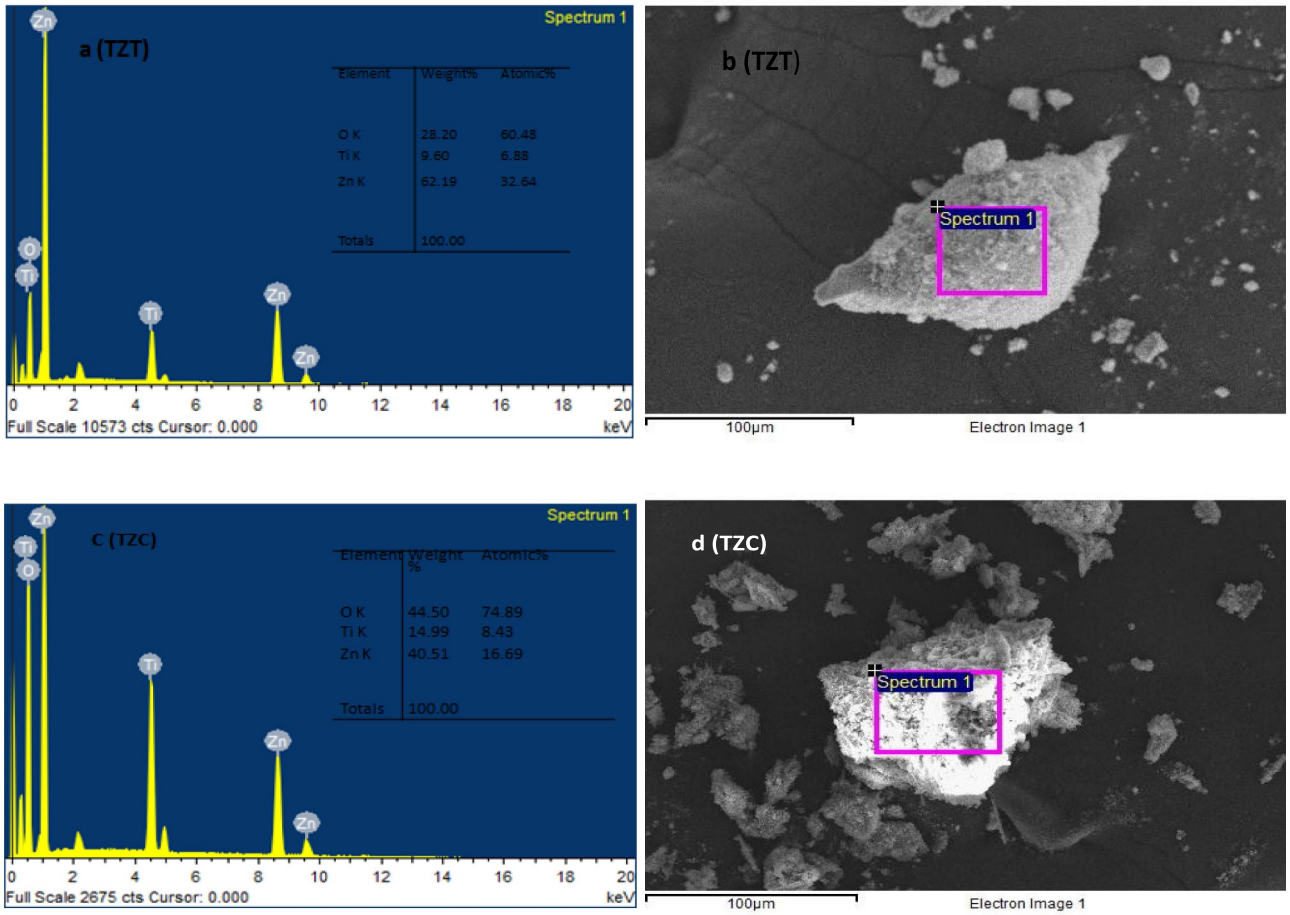

Fig.3 EDX images of TZC and TZT photocatalysts

No. 36–1451). The identified diffraction peaks are in accordance with existing literature [37]. The presence of narrow and intense diffraction peaks in the XRD pattern indicates the high crystallinity of the nanophotocatalysts [38]. Moreover, the existence of supplementary peaks at 25.3 and 48.05, °, 55.28°, and 62.7° degrees, corresponding to the diffraction planes (101) and (200), (2011) and (204) respectively, signifies the presence of the anatase phase of TiO_2 within the analyzed sample [39–41]. Nevertheless, the identification of three minor crystal peaks at 2θ values of 37.7, corresponding to the crystalline planes of (011), respectively, suggests the presence of a limited amount of rutile phase (JCPDS No. 80514) in the samples. It is noteworthy that these peaks align with the characteristic peaks of the anatase phase. Intriguingly, the same anatase peaks were also evident in the XRD pattern of pure TiO_2 with JCPDS No. 21.1272 in agreement with the literature [42]. There are two additional peaks in TZC patterns at 2 theta 27.45 (110) and 44.5 (210) indicating rutile phase.The appearance of rutile peaks at 2θ values of 37.7° (011) in the TZT pattern is likely due to calcination during the doping process, as the synthesized TiO_2 initially exhibited a pure anatase phase.

Table 1 summarizes the average crystallite sizes of TiO_2, TZT, and TZC photocatalysts, which were determined using the Debye–Scherrer Eq. (3).

$$d = \frac{K\lambda}{\beta \cos\theta} \tag{3}$$

In Eq. 2, *d* represents the crystallite size, λ denotes the wavelength of the incident X-ray, β is the full width at half maximum (FWHM) of the diffraction peak, *K* is the Scherrer constant (commonly 0.94), and θ refers to the scattering angle.

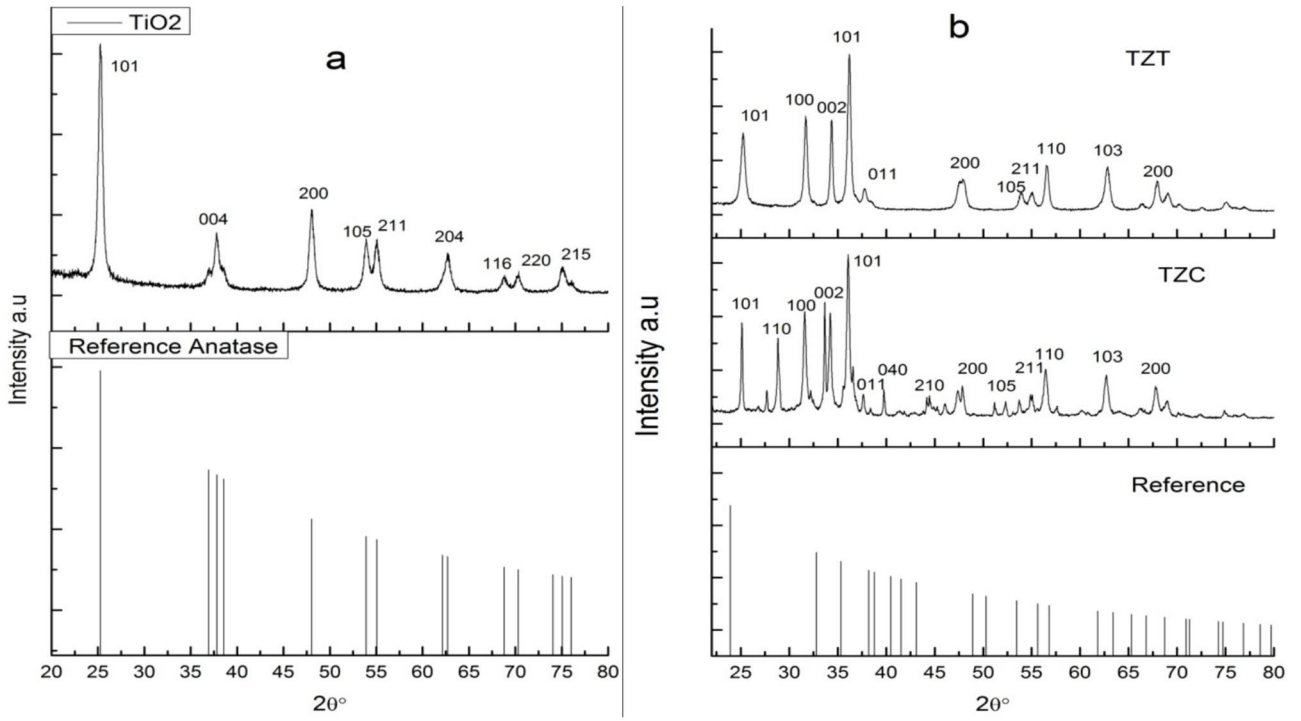

Fig.4 XRD patterns of **a** TiO_2 and **b** TZT, TZC photocatalysts

Table 1 Crystal's size of the photocatalysts

Photocatalyst type	TiO_2	TZC	TZT
Crystal size	14.83	21.4	21.3

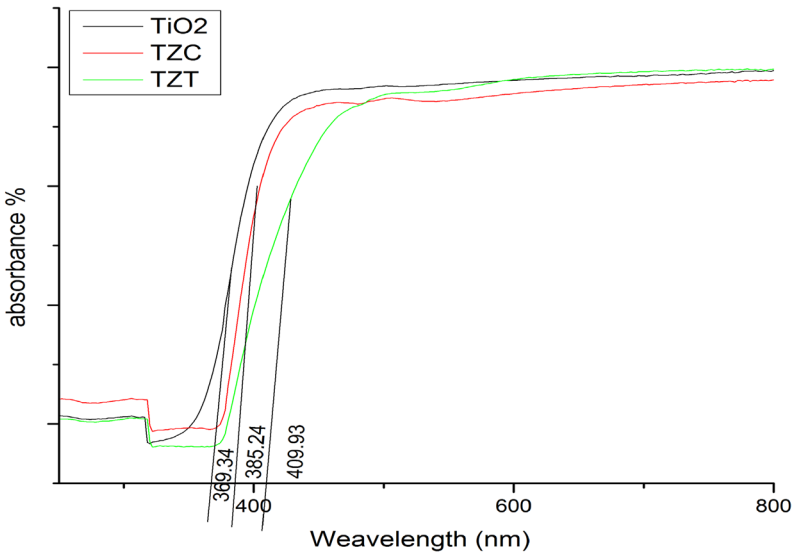

Fig.5 UV-DRS curves of TZT, TZC, and TiO_2 photocatalysts

3.1.4.1 UV DRS analysis In Fig. 5, the diffuse reflectance spectra (DRS) obtained from 200 to 800 nm for DRS TiO_2, TZC, and TZT photocatalysis reveal optical absorption peaks at wavelengths of 369.34 nm, 385.24 nm, and 409.93 nm, respectively. The bandgap energy (Eg) for each sample was determined using Eq. (4):

$$Eg = \frac{hc}{\lambda} \tag{4}$$

Here, h represents the Planck constant ((h = 4.14 × 10^{-15} eV. s), c is the speed of light (c = 2.99 × 10^{8} m/s), and λ is the wavelength of light.

The calculated energy bandgap values were 3.36eV, 3.22eV, and 3.02eV for TiO_2, TZC, and TZT photocatalysis, respectively. The outcomes indicate an increase in wavelength attributed to the incorporation of TiO_2 into ZnO. This change in band gap is indicative of the impact of the doping process on the optical properties of the synthesized nanoparticles. Notably, the reduction in band gap is anticipated to enhance catalytic activity. The results agree with the literature [5].

3.1.4.2 The porous structure analysis The surface area of TiO_2-ZnO photocatalyst materials is influenced by the thermal treatment process. For samples calcined at temperatures between 500 and 600 °C, the surface area ranges from 6.7 to 9.4 m^2/g [43, 44].

3.2 Degradation reaction of reactive blue dye under visible light irradiation

3.2.1 Degradation mechanism

The study targeted the photodegradation of reactive blue dye which is typically challenging to treat with traditional wastewater treatment methods [5, 7]. The mechanism of photocatalytic degradation involves the absorption of light by a semiconductor which excites electrons to move from the valence band to the conduction band. Dissolved oxygen serves as an electron acceptor leading to the formation of superoxide ($O_2^{\bullet-}$) and hydroperoxide ions (HO_2^-) and eventually hydroxyl (·OH) radicals. The holes in the valence band may also react with water molecules or hydroxide ions to produce the ·OH radicals [36] (Fig. 6). The photodegradation of the reactive blue dye using TiO_2-ZnO photocatalysts involves the generation of reactive oxygen species (ROS) through a sequence of photophysical and chemical reactions. These reactions occur as follows in Eqs. (5–11).

When TiO_2-ZnO is exposed to light with energy equal to or greater than its bandgap, electrons in the valence band (VB) are excited to the conduction band (CB), leaving behind positively charged holes in the VB

$$TiO_2 + ZnO + hv \rightarrow h^+ + e^- \tag{5}$$

The photogenerated electrons (e^-) and holes (h^+) interact with water and dissolved oxygen to produce reactive species:

3.2.1.1 Reduction of oxygen Electrons reduce oxygen molecules (O_2) into superoxide radicals (O_2^-•):

$$O_2 + e^- \rightarrow O_2^{\bullet-} \tag{6}$$

3.2.1.2 Formation of hydroperoxyl radicals The superoxide radicals react with protons (H^+) to form hydroperoxyl radicals (OOH•)

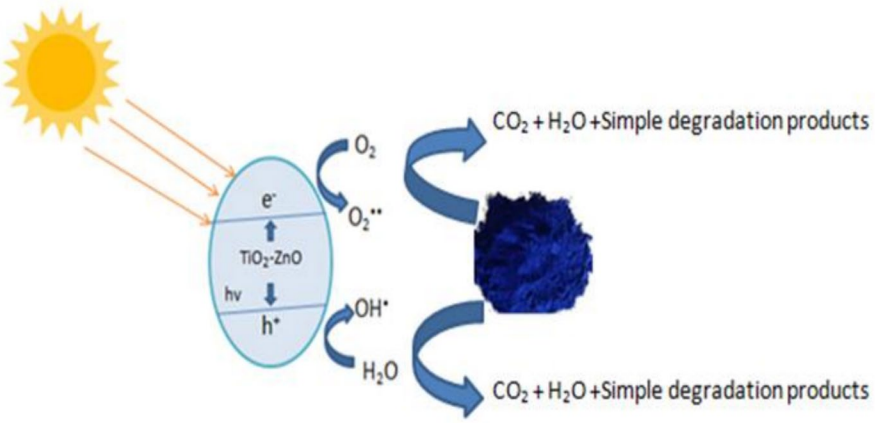

Fig. 6 Degradation mechanism of the reactive blue dye under sunlight irradiation

$$O_2^{\bullet -} + H^+ \rightarrow OOH^{\bullet} \quad (7)$$

3.2.1.3 Hydrogen peroxide and hydroxyl radicals Hydroperoxyl radicals and superoxide radicals combine or undergo further reactions to generate hydrogen peroxide (H_2O_2) and hydroxyl radicals (•OH)

$$2OOH^{\bullet} \rightarrow O_2 + H_2O_2 \quad (8)$$

$$e^- + H_2O_2 \rightarrow \bullet OH + OH^- \quad (9)$$

3.2.1.4 Oxidation of water by holes The photogenerated holes oxidize water molecules or hydroxide ions directly to form hydroxyl radicals:

$$h^+ + H_2O \rightarrow \bullet OH + H^+ \quad (10)$$

The reactive blue dye is oxidized and mineralized by the ROS and photogenerated holes

$$Reactive\ Blue + (e^-, H^+, OOH^{\bullet}, OH^{\bullet}, or\ O_2^{\bullet}-)) \rightarrow CO_2 + H_2O + simple\ degradation\ product \quad (11)$$

3.2.1.5 Effect of initial dye concentration In Fig. 7, the effect of initial dye concentration on photodegradation is illustrated. The final concentrations of the dye were 84%, 81.5%, and 81.3% for TiO_2 and 87%, 84%, and 82% for TZC for 1, 2, and 3 mg/l concentration of blue dye, respectively; and 100% removal efficiency for the three concentrations of dye using TZT. As the blue dye concentration increases, the degradation efficiency decreases due to the reduction in catalyst activity caused by the heightened presence of adsorbed compounds on the catalyst's surface [5]. The removal efficiency of TZT was higher than TZC and reached 100%. This was attributed to the lower band gap (shift towards visible light region) of TZT (3.02eV) compared to that of TZC (3.22eV) and TiO_2 (3.36eV). This shift resulted in absorption of visible light as confirmed by UV DRS results. The high performance of TZT can also be attributed to its unique characteristics such as smaller crystallite size compared with TZC (Table 1) and surface properties (Fig. 3). Additionally, the k-values of TZT powders were significantly higher than those of TZC and bare TiO_2 (Sect. (3.2.6)). All these attributes resulted in superior performance due to photo-induced electron trapping effect of TZT, enhanced OH radicals on its surface, and smaller crystallite size [45, 46].

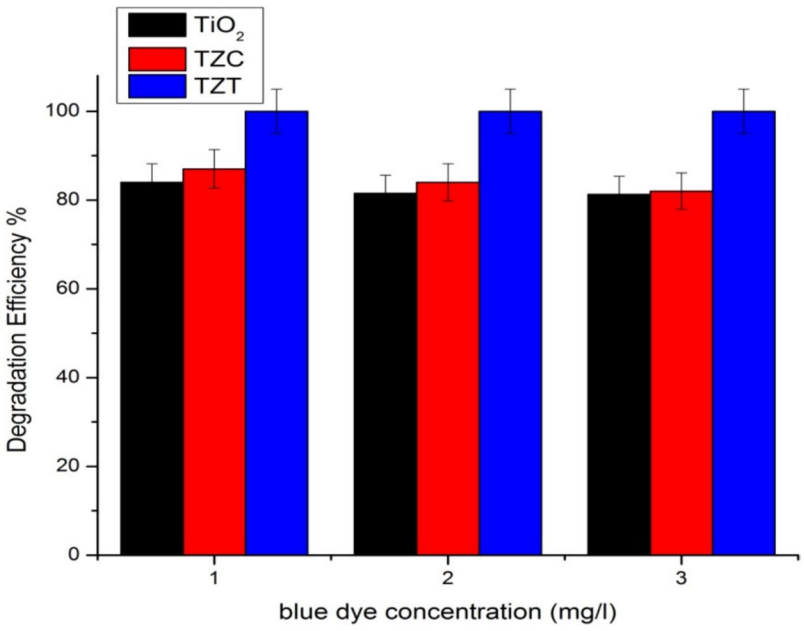

Fig. 7 Reactive blue dye degradation efficiency % using TiO_2, TZC, and TZT photocatalysts at (1mg/l, 2mg/l, and 3mg/l) concentrations of the blue dye after 2 h irradiation time

3.2.1.6 Effect of reaction contact time Figure 8 shows the effect of reaction contact time on the degradation efficiency. There was a direct correlation between degradation and irradiation time. Increasing sunlight radiation time enhances the sensitivity of photocatalyst nanoparticles. This is because longer exposure to sunlight leads to a greater number of electrons moving from the valence band to the conduction band, thereby increasing the generation of electron–hole pairs [29, 47]. The utilization of a solar concentrator further contributes to the degradation process. The degradation efficiency for TiO_2 (Fig. 8a) enhanced from (68, 69, 65) % to (84, 81.5, 81.3) % and for TZC (Fig. 8b) improved from (68, 67.7, and 65.2) % to (87, 84, and 82) % for 1, 2, and 3mg/l blue dye, respectively as irradiation time was increased from 1 to 2 h. Whereas using TZT (Fig. 8c), the performance improved from (95, 93, 48, and 91) % to 100% after 2 h for all the concentrations of reactive blue dye. This demonstrated the efficacy of the synthesized TiO_2 doped ZnO nanocatalyst (TZT) in the degradation process.

3.2.1.7 Effect of photocatalysis dose TiO_2 nanoparticles (NPs) showed excellent photocatalytic activity (Fig. 9a), with dye removal efficiency increasing as the concentration of TiO_2-ZnO increased. This improvement is attributed to greater electron–hole pair formation, where the resulting holes interact with water and hydroxyl anions to generate hydroxyl radicals [29, 48].

In the case of TiO_2-ZnO photocatalysts (Fig. 9b, c), the results revealed even higher photocatalytic performance. Doping TiO_2 with ZnO shifts the bandgap energy toward the visible light spectrum, allowing better sunlight

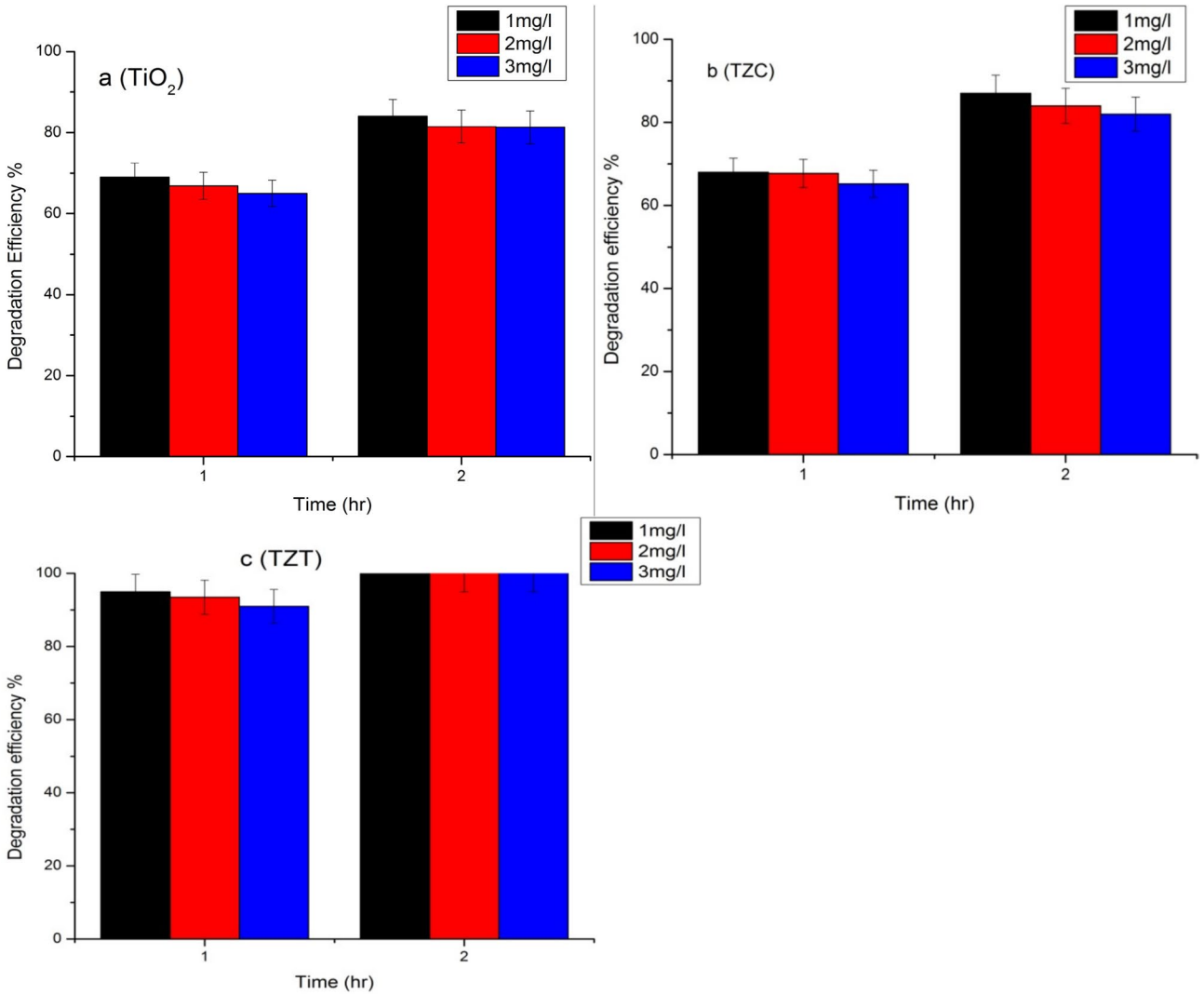

Fig.8 Degradation efficiency % of blue dye by **a** TiO_2, **b** TZC, and **c** TZT photocatalyst using 1mg/l, 2mg/l, and 3mg/l photocatalysis concentration for 2 h irradiation time

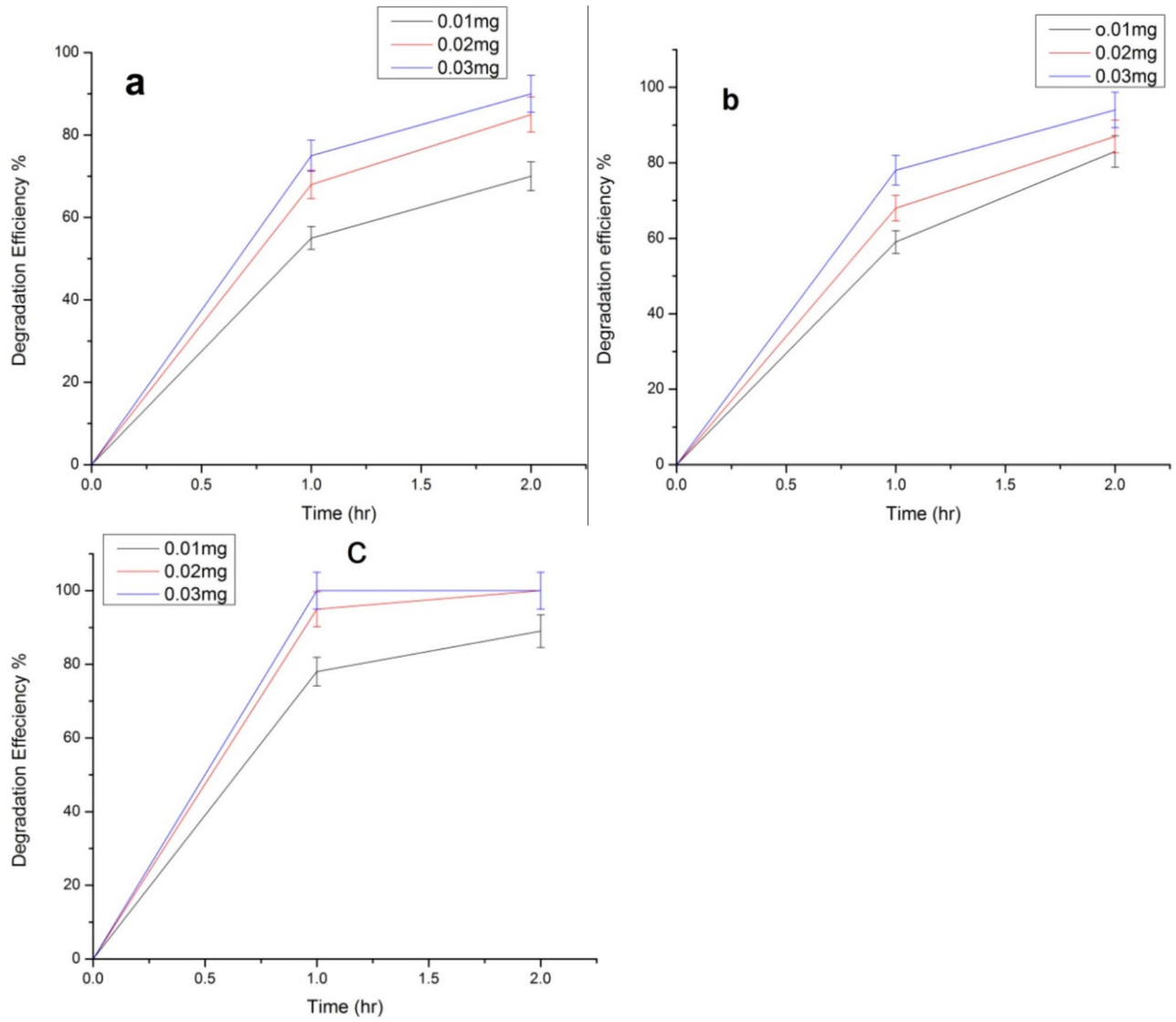

Fig. 9 Reactive blue dye (1mg/l) degradation efficiency using (0.01–0.03mg) of **a** TiO_2, **b** TZC and **c** TZT photocatalysts

absorption and enhancing the production of hydroxyl radicals [49]. Under optimal conditions, with a concentration of 3 mg/L for each photocatalyst, ZnO alone achieved 87% dye degradation after 1 h, improving to 90% after 2 h. For the codoped photocatalysts, TZC reached 75% degradation after 1 h and 92% after 2 h, while TZT achieved 99% after 1 h and complete 100% removal after 2 h of irradiation.

3.2.1.8 Effect of solution pH This study explores the impact of pH on the photocatalytic degradation of Reactive Blue dye using bare TiO_2 and co-doped photocatalysis TZC and TZT. The pH range of 5 to 9 was tested (Fig. 10), showing that acidic and neutral pH levels were more effective for dye degradation than basic conditions. At lower pH (below 6.8), the photocatalysis are positively charged, favoring the adsorption of negatively charged dye molecules due to electrostatic attraction, which enhances degradation efficiency [25]. At pH 7, full degradation was still achieved for TZT, primarily driven by hydroxyl radicals in the bulk solution. However, at higher pH levels (above 7), photocatalysis becomes negatively charged, leading to electrostatic repulsion between TiO_2 and the dye molecules. This repulsion reduces adsorption, slowing down degradation. Additionally, hydroxyl radicals are scavenged by superoxide ions and other species, further decreasing the efficiency [50].

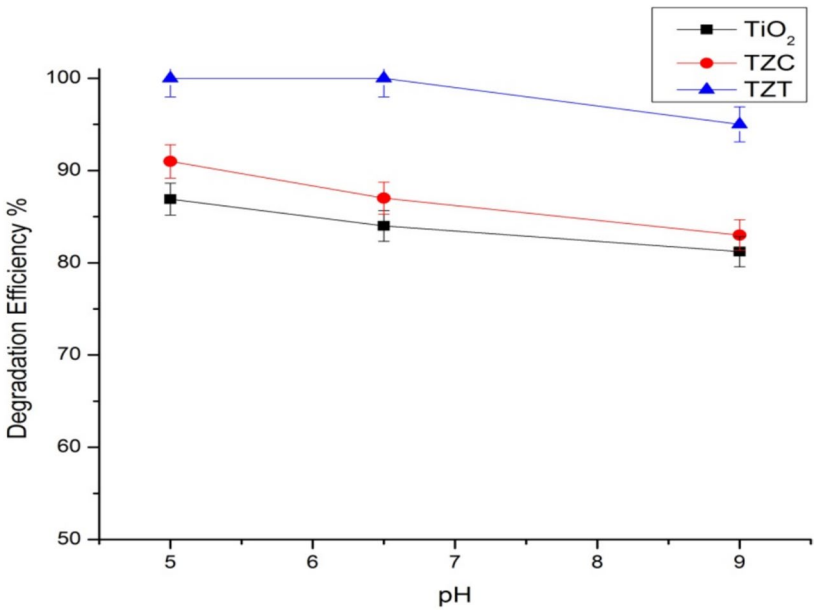

Fig. 10 Reactive blue dye (1mg/l) degradation efficiency using solution pH (5–9) and 0.03 mg of TiO_2, TZC and TZT photocatalysts

3.2.1.9 Kinetic analysis of photocatalytic degradation The plots of $\ln(C/C_{0})$ versus reaction time for bare TiO_2 and the doped photocatalysts (TZC and TZT) are shown in Figs. 11a–c, respectively. These plots were obtained under the optimal reaction conditions: a blue dye concentration of 1 mg/L, a photocatalyst dose of 0.03 g/L, and a pH of 5. The rate constants (k) were calculated from the slopes of these plots.

Figure 11 clearly illustrates that doping significantly enhances the reaction rate. Furthermore, the use of synthetic TiO_2 in the doped photocatalysts outperformed the commercial TiO_2 counterpart in terms of photocatalytic activity. The calculated k values for bare TiO_2, TZC, and TZT photocatalysts were 0.01203, 0.01511, and 0.08261 min^{-1}, respectively. These results confirm that doping and the synthesis method play crucial roles in improving the photocatalytic efficiency.

3.2.1.10 Photocatalyst stability The stability of a photocatalyst is a critical factor for its practical application. The findings from the stability study, illustrated in Fig. 12, highlight the activity and durability of the TiO_2-ZnO photocatalysts (TZT and TZC) over five consecutive cycles of reactive blue dye degradation. The results revealed minimal decreases in degradation efficiency after five successive runs, underscoring the significant stability and activity of both photocatalysts. Notably, the degradation percentages remained consistent, with no substantial changes observed for either TZT or TZC photocatalysis. However, a slight reduction in efficiency was attributed to the potential loss of catalyst material during the filtration process [51]. A comparative analysis demonstrated that TZT exhibited superior stability compared to TZC. The degradation efficiency of TZT decreased by only 6%, whereas TZC showed a 9% reduction, as depicted in Fig. 12. This enhanced stability of TZT can be attributed to the high purity of the synthesized TiO_2. Despite the minor decrease in efficiency, both photocatalysts confirmed their significant activity and robustness, making them promising candidates for the degradation of reactive blue dye.

The study demonstrated the high efficiency of TiO_2-doped ZnO photocatalysts, which significantly enhanced the bandgap energy. This improvement allowed the doped photocatalysts to effectively absorb sunlight, activate the photocatalytic process, and degrade the blue dye. The results, as presented in Table 2, highlight the superior performance of this photocatalyst compared to those reported in other studies.

4 Conclusions

In this study, successful degradation of blue dye in water solutions was accomplished. The ZnO-TiO_2 photocatalysts were synthesized using both commercial and synthesized TiO_2 from TTIP precursor. Comparative analysis revealed that ZnO-TiO_2 photocatalysts from synthetic TiO_2 exhibited superior properties when contrasted with ZnO-TiO_2 photocatalysts from commercial TiO_2 and bare TiO_2. This enhancement was primarily attributed to shifts in absorbance from the UV to the visible region, as verified by UV DRS analysis. Photocatalysis experiments involving TiO_2, TZC, and TZT demonstrated

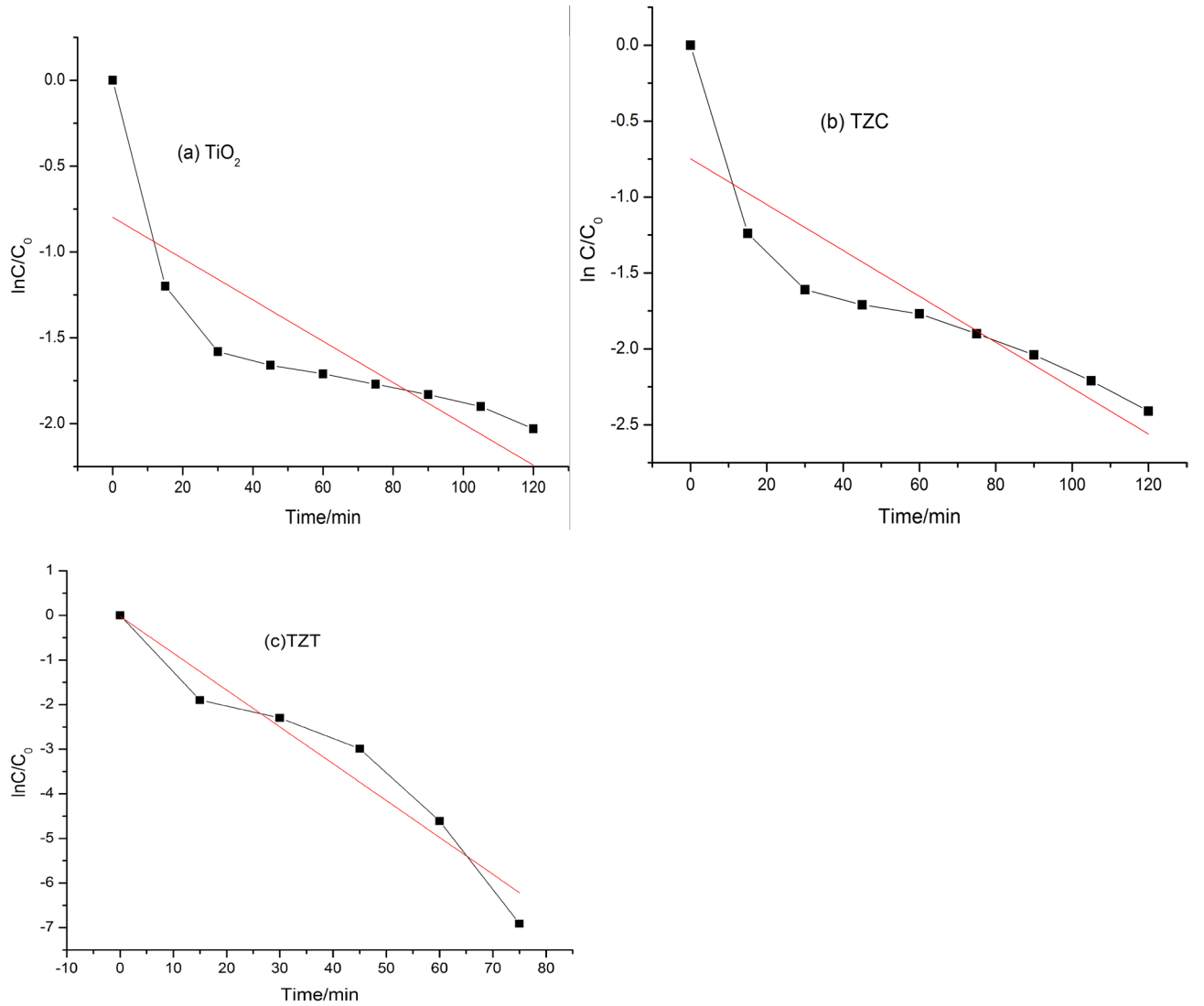

Fig. 11 plot of ln (C/C_0) Vs time using **a** TiO_2, **b** TZC, and **c** TZT photocatalysis

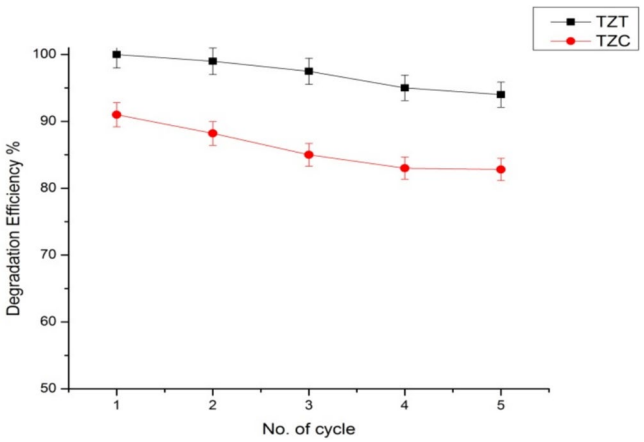

Fig. 12 Stability study of TZT and TZC photocatalysis over 5 cycles

Table 2 Reported studies on photo-degradation of organic dye

Photocatalyst type	Photocatalyst-Dosage (g/l)	Time/min	Type of dye	Source of light	Removal efficiency **(%)**	Ref
TiO_2–Fe_2O_3	0.04	120	Navy blue 171	sunlight	100	[32]
graphitic carbon nitride	3	320	Rhodamine B	sunlight	95	[52]
Cu-complex	0.4	40	Methylene blue	UV light	70.71	[53]
ZnO	0.01–0.06	20	Reactive blue 203	8W UV lamp	99.1	[29]
TiO_2	1	120	Procion Navy H-EXL (PN)	UV-LED	100	[54]
TiO_2–ZnO	0.03	120	Navy blue 171	sunlight	100	Present work

optical absorption peaks at wavelengths of 369.34 nm, 385.24 nm, and 409.93 nm, respectively, demonstrating a progressive shift in light absorption to the visible region for TZT more than TZC. The dye removal efficiency increased with increasing contact time and the photocatalysis dosage. While it decreased with higher initial dye concentrations. In this study the optimum condition was achieved using 1 mg/l dye concentration with 0.03 mg photocatalysis and 5 pH solution for 2 h sunlight irradiation time. However, the ZnO-TiO_2 photocatalyst synthesized from titanium precursor, achieved 100% removal efficiency for all dye concentrations investigated. The rate constants (k) were 0.01203, 0.01511, and 0.08261 min^{-1} for bare TiO_2, TZC, and TZT photocatalysts, respectively. The TiO_2-ZnO photocatalysts (TZT and TZC) were recovered and reused over five consecutive cycles of reactive blue dye degradation, thus demonstrating the stability and durability. The study demonstrated the effectiveness of TiO_2-ZnO photocatalysts under solar radiation to effectively degrade reactive blue dye. Following the promising results obtained. This study utilized a single concentration of TiO_2 and zinc acetate in synthesizing the doped TiO_2-ZnO (50:50). Further research is recommended to explore the effects of varying co-doping ratios of TiO_2 and zinc acetate, as well as to assess the efficiency of the photocatalysts in degrading different dyes and other organic contaminants.

Acknowledgements This work was supported by European commission (EU) through Strengthening mobility and promoting Regional Integration in Engineering Education in Africa (SPREE) program (Grant numbers 614586-mobaf-20191-1).

Author contributions Zeinab A. Suliman, Achisa C. Mecha, and Josphat I. Mwasiagi wrote the main manuscript text and Zeinab A. Suliman prepared figures and lab working. Achisa C. Mecha and Josphat I. Mwasiagi Visualization, Supervision, and Conceptualization. All authors reviewed the manuscript.

Data availability The datasets generated during and/or analyzed during the current study are available from the corresponding author on reasonable request.

Declarations

Competing interests The authors declare no competing interests.

References

1. Bekele SG, Ganta DD, Endashaw M. Green synthesis and characterization of zinc oxide nanoparticles using Monoon longifolium leave extract for biological applications. Dis Chem. 2024;1(1):5.
2. Song X, et al. Fracture of magnesium matrix nanocomposites-a review. Int J Lightweight Mater Manuf. 2021;4(1):67–98.
3. Yaqoob AA, et al. Role of nanomaterials in the treatment of wastewater: A review. Water. 2020;12(2):495.
4. Saravanan A, et al. Effective water/wastewater treatment methodologies for toxic pollutants removal: Processes and applications towards sustainable development. Chemosphere. 2021;280: 130595.

5. Alizadeh E, Baseri H. Photocatalytic degradation of sumatriptan succinate by ZnO, Fe doped ZnO and TiO_2-ZnO nanocatalysts. Mater Chem Horizons. 2022;1(1):7–21.
6. Ahamad T, et al. Fabrication of MoS_2/ZnS embedded in N/S doped carbon for the photocatalytic degradation of pesticide. Mater Lett. 2020;263: 127271.
7. Benhebal H, et al. Photocatalytic degradation of phenol and benzoic acid using zinc oxide powders prepared by the sol–gel process. Alex Eng J. 2013;52(3):517–23.
8. Abbasi A, et al. Photo-degradation of methylene blue: photocatalyst and magnetic investigation of Fe_2O_3–TiO_2 nanoparticles and nanocomposites. J Mater Sci Mater Electron. 2016;27:4800–9.
9. Kumar MA, et al. Enhanced photocatalytic and electrochemical performance of TiO_2-Fe_2O_3 nanocomposite: Its applications in dye decolorization and as supercapacitors. Sci Rep. 2020;10(1):1249.
10. Shathy RA, et al. Natural sunlight driven photocatalytic removal of toxic textile dyes in water using B-doped ZnO/TiO_2 nanocomposites. Catalysts. 2022;12(3):308.
11. Bhanvase B, Shende T, Sonawane S. A review on graphene–TiO2 and doped graphene–TiO_2 nanocomposite photocatalyst for water and wastewater treatment. Environ Technol Rev. 2017;6(1):1–14.
12. Karume I, et al. Impact of synthetic method and metal type on the efficiency of metal-based nanoparticles against pathogens and chemical pollutants. Dis Chem. 2024;1(1):1–13.
13. Al Zoubi W, et al. A review on TiO_2-based composites for superior photocatalytic activity. Rev Inorg Chem. 2021;41(4):213–22.
14. Leary R, Westwood A. Carbonaceous nanomaterials for the enhancement of TiO_2 photocatalysis. Carbon. 2011;49(3):741–72.
15. Yang X, et al. Synthesis of visible-light-active TiO_2-based photocatalysts by carbon and nitrogen doping. J Catal. 2008;260(1):128–33.
16. Aremu O, et al., Synthesis and applications of nano-sized zinc oxide in wastewater treatment: a review. International Journal of Environmental Science and Technology, 2021: p. 1–20.
17. Shekofteh-Gohari M, et al. Magnetically separable nanocomposites based on ZnO and their applications in photocatalytic processes: a review. Crit Rev Environ Sci Technol. 2018;48(10–12):806–57.
18. Rheima, A.M., D.H. Hussain, and H.J. Abed. *Fabrication of a new photo-sensitized solar cell using TiO_2\ZnO Nanocomposite synthesized via a modified sol-gel Technique*. in *IOP Conference Series: Materials Science and Engineering*. 2020. IOP Publishing.
19. Munguti L, Dejene F. Influence of annealing temperature on structural, optical and photocatalytic properties of ZnO–TiO_2 composites for application in dye removal in water. Nano-Structures & Nano-Objects. 2020;24: 100594.
20. Ramírez-Ortega D, et al. Semiconducting properties of ZnO/TiO_2 composites by electrochemical measurements and their relationship with photocatalytic activity. Electrochim Acta. 2014;140:541–9.
21. Nemiwal M, Zhang TC, Kumar D. Recent progress in g-C3N4, TiO_2 and ZnO based photocatalysts for dye degradation: Strategies to improve photocatalytic activity. Sci Total Environ. 2021;767: 144896.
22. Karthikeyan C, et al. Recent advances in semiconductor metal oxides with enhanced methods for solar photocatalytic applications. J Alloy Compd. 2020;828: 154281.
23. Ali MM, et al. Nano synthesis of ZnO–TiO_2 composites by sol-gel method and evaluation of their antibacterial, optical and photocatalytic activities. Results Mater. 2021;11: 100199.
24. Liu S. Graphene oxide and graphene based catalysts in photochemical ractions. New York: Curtin University; 2013.
25. Samsudin EM, et al. Evaluation on the photocatalytic degradation activity of reactive blue 4 using pure anatase nano-TiO_2. Sains Malaysiana. 2015;44(7):1011–9.
26. Kaur N, Shahi SK, Singh V. Anomalous behavior of visible light active TiO_2 for the photocatalytic degradation of different Reactive dyes. Photochem Photobiol Sci. 2015;14:2024–34.
27. Lucarelli L, Nadtochenko V, Kiwi DJ. Environmental photochemistry: quantitative adsorption and FTIR studies during the TiO_2-photocatalyzed degradation of orange II. Langmuir. 2000;16(3):1102–8.
28. Samuel JJ, Yam F. Photocatalytic degradation of methylene blue under visible light by dye sensitized titania. Mater Res Express. 2020;7(1): 015051.
29. Bagheri M, Najafabadi NR, Borna E. Removal of reactive blue 203 dye photocatalytic using ZnO nanoparticles stabilized on functionalized MWCNTs. J King Saud Univ Sci. 2020;32(1):799–804.
30. Bouziani A, Park J, Ozturk A. Synthesis of α-Fe_2O_3/TiO_2 heterogeneous composites by the sol-gel process and their photocatalytic activity. J Photochem Photobiol A. 2020;400: 112718.
31. Yadav A, Hunge Y, Kang S-W. Porous nanoplate-like tungsten trioxide/reduced graphene oxide catalyst for sonocatalytic degradation and photocatalytic hydrogen production. Surf Interfaces. 2021;24: 101075.
32. Suliman ZA, Mecha AC, Mwasiagi JI. Effect of TiO_2/Fe_2O_3 nanopowder synthesis method on visible light photocatalytic degradation of reactive blue dye. Heliyon. 2024. https://doi.org/10.1016/j.heliyon.2024.e29648.
33. Laid N, et al. Characterization of ZnO and TiO_2 Nanopowders and their Application for Photocatalytic Water Treatment. Acta Physica Polonica A. 2020;137(3):305.
34. Hussain ST, Khan K, Hussain R. Size control synthesis of sulfur doped titanium dioxide (anatase) nanoparticles, its optical property and its photo catalytic reactivity for CO_2+ H_2O conversion and phenol degradation. J Nat Gas Chem. 2009;18(4):383–91.
35. Mandzy N, Grulke E, Druffel T. Breakage of TiO_2 agglomerates in electrostatically stabilized aqueous dispersions. Powder Technol. 2005;160(2):121–6.
36. Khan MAN, et al. Removal of reactive blue 19 dye by sono, photo and sonophotocatalytic oxidation using visible light. Ultrason Sonochem. 2015;26:370–7.
37. Ma H et al. *Synthesis, characterization, and photocatalytic activity of N-doped ZnO/ZnS composites.* International Journal of Photoenergy, 2013. **2013**(625024,): p. 8.
38. Sharma S, Mehta S, Kansal S. N doped ZnO/C-dots nanoflowers as visible light driven photocatalyst for the degradation of malachite green dye in aqueous phase. J Alloy Compd. 2017;699:323–33.
39. Abdel-Wahab A-M, et al. Photocatalytic degradation of paracetamol over magnetic flower-like TiO_2/Fe_2O_3 core-shell nanostructures. J Photochem Photobiol A. 2017;347:186–98.

40. Ijadpanah-Saravy H, et al. Synthesis of titanium dioxide nanoparticles for photocatalytic degradation of cyanide in wastewater. Anal Lett. 2014;47(10):1772–82.
41. Theivasanthi T, Alagar M, Titanium dioxide (TiO_2) nanoparticles XRD analyses: an insight. arXiv preprint arXiv:1307.1091, 2013.
42. Khasawneh OFS, et al. Removal of acetaminophen using Fe_2O_3-TiO_2 nanocomposites by photocatalysis under simulated solar irradiation: Optimization study. J Environ Chem Eng. 2021;9(1):104921.
43. Siwińska-Stefańska K, et al. TiO_2-ZnO binary oxide systems: comprehensive characterization and tests of photocatalytic activity. Materials. 2018;11(5):841.
44. Lin S, Songyuan L, Yaochong F. Facile preparation of ZnO/TiO_2 nanocomposite photocatalysts and study of their photocatalytic performance. J Ovonic Res. 2023;19(6):739.
45. Sangchay W, Sikong L, Kooptarnond K. Comparison of photocatalytic reaction of commercial P25 and synthetic TiO_2-AgCl nanoparticles. Proc Eng. 2012;32:590–6.
46. Castilhos S, et al. Assessment comparison of commercial TiO_2 and TiO_2 sol-gel on the degradation of caffeine using artificial radiation. Environ Sci Pollut Res. 2020;27:22155–68.
47. Barakat M, et al. Photocatalytic degradation of 2-chlorophenol by Co-doped TiO_2 nanoparticles. Appl Catal B. 2005;57(1):23–30.
48. Ghaderi A, Abbasi S, Farahbod F. Synthesis of SnO2 and ZnO nanoparticles and SnO_2-ZnO hybrid for the photocatalytic oxidation of methyl orange. Iran JChem Eng. 2015;12(3):96–105.
49. Navidpour AH, et al. Immobilization of TiO_2 and ZnO by facile surface engineering methods to improve semiconductor performance in photocatalytic wastewater treatment: A review. Mater Sci Semicond Process. 2024;179: 108518.
50. Marcelo CR, et al. Degradation of the reactive blue 4 dye in aqueous solution using zero-valent copper nanoparticles. J Nanomater. 2018;2018:1–9.
51. Hunge YM, et al. Visible light-assisted photocatalysis using spherical-shaped bivo4 photocatalyst. Catalysts. 2021;11(4):460.
52. Yadav A, Kang S-W, Hunge Y. Photocatalytic degradation of Rhodamine B using graphitic carbon nitride photocatalyst. J Mater Sci: Mater Electron. 2021;32(11):15577–85.
53. Jamil M, et al. Photocatalytic degradation of methylene blue dye and electrocatalytic water oxidation over copper (II) complex with mixed ligands. J Photochem Photobiol A. 2024;446: 115095.
54. Tapia-Tlatelpa T, Trull J, Romeral L. In situ decolorization monitoring of textile dyes for an optimized UV-LED/TiO_2 reactor. Catalysts. 2019;9(8):669.